November 1985 LRP 270/85

A PRELIMINARY STUDY OF ALFVEN WAVE HEATING FOR ASDEX UPGRADE

G.A. Collins, F. Hofmann and J.B. Lister

A PRELIMINARY STUDY OF ALFVEN WAVE HEATING FOR ASDEX UPGRADE

G.A. Collins, F. Hofmann and J.B. Lister

Centre de Recherches en Physique des Plasmas
Association Euratom - Confédération Suisse
Ecole Polytechnique Fédérale de Lausanne
21, av. des Bains - 1007 Lausanne/Switzerland

Abstract

It is interesting to study the possibility of applying Alfvén Wave Heating (AWH) to a large tokamak, ASDEX Upgrade. We give a rapid review of AWH including the major outstanding questions. The spectra for typical ASDEX Upgrade conditions are presented together with preliminary estimates of the loading expected using the proposed ICRH antennae. We find that these antennae could produce interesting results although they have not been at all optimized for AWH. The off-torus tuned circuit and power supplies would present no technological difficulties. Only a minor technical design constraint - a higher current capability for the antenna feeds - would permit AWH experiments to be carried out on ASDEX Upgrade at high power.

I. INTRODUCTION

This report is intended as a study of the implications of AWH for ASDEX Upgrade. It is limited to a discussion related to AWH using the planned ICRH antennae, with no optimisation of antenna design for the lower frequency range. It is intended to carry out a second study, a fully optimised design in the available space, subsequently if requested.

In Section II we give a very brief outline of AWH physics, including the most important outstanding questions. In Section III we look at the spectrum and antenna loading for AWH in ASDEX Upgrade. In Section IV we consider an antenna layout which is not toroidally periodic, followed by a conceptual antenna circuit in Section V. Section VI discusses the power and generator requirements. In Section VII we discuss the implications for ASDEX Upgrade of leaving open the possibility of carrying out AWH using the ICRH antennae. In Section VIII we draw some conclusions.

II. PHYSICS SUMMARY

II.1 Theoretical Basis

Alfvén Wave Heating generally refers to the resonant absorption and subsequent conversion of a wave's energy in a non-uniform plasma where the imposed wave's phase-velocity equals the local value of the Alfvén velocity. The Shear Alfvén resonance is the major absorption mechanism available at frequencies below the ion cyclotron frequency, ω_{ci}.

Antennae external to the plasma create magnetic field and hence pressure modulations which are arranged to have both a definite frequency and a definite wavelength. Theory and experiment have both demonstrated an improved loading of the antenna structure when it excites the so-called "surface wave". This is the first radial eigenmode of the asymmetrical ($m \neq 0$) fast wave in a plasma column surrounded by a vacuum layer, and is heavily damped at any Alfvén resonance layer.

The resonance frequency for the Shear Alfvén Wave is given, in the cylindrical approximation, by

$$f^2 = \frac{B_\phi^2 (n+m/q(r))^2}{\mu_0 \rho(r) (2\pi R_0)^2} \cdot (1 - \omega^2/\omega_{ci}^2) \qquad (1)$$

where n and m are the toroidal and poloidal wavenumbers respectively. This frequency can be rewritten as

$$f(MHz) = \frac{B_\phi(T)(n+m/q(r))}{R_0\sqrt{<A>n_{el3}(r)}} \times (1 - \omega^2/\omega_{ci}^2)^{1/2} \times 1.1 \qquad (2)$$

where

$$\omega/\omega_{ci} = \frac{f(MHz)}{B_\phi(T)} \times \frac{<A>}{<Z>} \times 0.066 \qquad (3)$$

The radial profile of this resonance frequency depends on the values of n and m and on the q- and density profiles. The position of the dominant resonance surface is slightly shifted towards the centre in toroidal geometry compared with its value given by a cylindrical calculation.

II.2 Experimental Status - antenna characteristics

In the EEC there is, at present, only one experiment on AWH, namely the TCA tokamak in Lausanne. Elsewhere in the world other tokamaks and stellarators study AWH, but we refer to the results of TCA with which we are most familiar.

The antenna system in TCA consists of eight groups of three antennae placed above and below the plasma, with two groups in each torus quadrant. They are electrically floating with respect to the torus, and are powered in parallel from a single oscillator using four commercial 360 kW water-cooled triodes giving a total power of 400 kW available as antenna loading. Experiments have been carried out between 2-6 MHz with most of the work carried out at 2.5 MHz. The pulse length is typically 30 msec. By separately phasing the antennae and paying careful attention to the current balancing we can vary the dominant toroidal and poloidal mode numbers.

The first low power experiments on TCA confirmed the parametric dependence of the loading predicted by MHD theory, and also revealed narrow resonances which appeared as peaks in the loading at frequencies just below the start of the continua associated with the Alfvén resonance layers. These resonances have been identified as global eigenmodes of the Alfvén wave, and we observed on TCA that these eigenmodes (or Discrete Alfvén Waves) only occur for one sign of helicity ($n/m > 0$). Unlike the continuum loading, their usefulness for heating depends on the damping mechanism, and, like the fast wave eigenmodes, they suffer from being natural modes of the plasma, with large wave amplitudes. The possibility of launching waves with a preferred toroidal direction has confirmed the DAWs to be dominantly excited in the direction of electron drift, i.e. with both m and n negative.

More recently we have shown a loading peak at the $(n,m) = (2,0)$ continuum threshold where there is no resonance layer excited in cylindrical geometry. Numerical codes have shown that the $(n,m) = (2,0)$ continuum is in fact excited by our antenna structure $(N,M) = (2,1)$ via toroidal coupling. It is therefore clear that for low n-numbers the recently increased understanding of toroidal coupling effects is important for interpreting the experimental results. A recent and detailed description of all these studies is to be found in Ref. [1].

II.3 Heating Studies on TCA

The higher power rf experiments show up several effects : an increase in ion temperature, an increase in electron temperature, an increase in plasma density, and an increase in the radiated power loss. We now very briefly discuss these various points. More details are to be found in the published results, Refs. [2-5].

II.3a) Impurity problems. The first experiments on TCA were plagued by impurity problems. We have introduced TiN-coated (6-7 μm) bar antennae instead of the original plate antennae and now use SiC-coated graphite limiters. In the presence of lateral screens the radiated power loss from the centre of the plasma was negligible, although the Z_{eff}

increased due to an increase of silicon contamination. Without the screens, there is still some metallic impurity contamination. The effect of, and optimal design of, the lateral screens, or indeed their necessity, are currently under investigation. The metallic impurity influx is however low enough to study clearly the electron energy balance.

II.3b) Density increase. During the rf pulse there is a considerable increase in electron density, up to 300% depending on the target plasma density and generally linear with rf power. We consider that this cannot be solely explained by impurity influx as it has withstood the various changes implemented and has shown a marked dependence on the structure of the resonance surfaces. We consider that a large part of the increase may be an effect of the presence of the wavefield. It is difficult to estimate the relative contributions from impurity influx, neutral recycling changes and particle confinement changes. There is usually a marked reduction in H_α emission during the rf pulse. Recent results are described in Ref. [6].

II.3c) Ion temperature. An ion temperature increase, corresponding to $\overline{n_e}\ \Delta T_i/P_{rf} \sim 1.5\text{-}14 \times 10^{13}$ eV/kW•cm^3 (in naive units), is observed during the rf pulse, and has been maintained throughout the various modifications. Typically the increase is from 300-600 eV. Its interpretation is confused by the increase in electron density and increase in Z_{eff}, but it cannot be fully explained without direct ion-heating. The mechanism for this is not established. The increase in ion temperature is maintained for the full length of the rf pulse, but is also dependent on the spectrum. The most recent results show discontinuous behaviour in ion heating when crossing a mode threshold, with anomalously strong ion heating observed below the threshold [7].

II.3d) Electron temperature. Even following the considerable improvements to the target plasma cleanliness, the electron temperature increase (up to $\overline{n_e}\ \Delta T_e/P_{rf} \sim 3\text{-}4 \times 10^{13}$ eV/kW•cm^3) is not maintained for the full 30 msec. This represents 5-10 energy confinement times, however, which is long compared with many other experiments.

The reasons for this subsequent decrease are still not clear, as the increase in radiated power loss is still large enough to be the sole cause. Again, it is difficult to separate time in the pulse and the change in density which causes a change in the spectrum excited. As well as the increase in average central temperature, to well above the ohmically heated level, we observe very strong sawtoothing behaviour and this is interpreted as a strongly peaked power deposition profile, as argued in Ref. [7].

II.4 Outstanding physics issues

Dissipation/wave conversion. At present no AWH work is underway on this topic in the EEC and reliance is placed on preliminary work by Chen and Hasegawa and more recently at Sydney and Texas. On the Kinetic Alfvén Wave in particular, since no database exists for present-day experiments, extrapolation of the dissipative mechanism to a larger device is a little tentative ! It might be expected that, at higher power densities, non-linear behaviour would be observed.

Antenna optimisation. The complexity of a full antenna system limits the number of experimental tests at present. Considerable reliance is therefore to be placed on theoretical models, justified by their good agreement with experiment (at least on TCA), to point the way to an optimised antenna. TCA will test more advanced antenna designs, including screens and tilted antennae.

Origins of the density increase. Most rf heating methods now confess to a density rise during the heating pulse. The origins of this effect (reduced losses, pump-in, impurity generation, change in recycling at the wall) are under study in TCA. The CRPP is presently studying the effects of resonant wave-particle interactions.

Increase in impurity concentration. The problems encountered in TCA are being resolved by limiter design, antenna design and screen design studies.

Related heating methods. Proposals have been made to use the global eigenmodes for plasma heating or to use, in large machines, the fast-

wave cavity modes as the energy carrier. At present there is no experimental information available concerning either proposal which would indicate any superiority over AWH in the continua using the surface wave as the energy carrier.

Position of the resonant surface. The importance of the radius of the resonant surface(s) has been shown via discontinuities in several observable parameters. It is not yet at all clear whether ultimately AWH will require that the resonant layer be reasonably central. Neither is it clear whether the electron and ion heating observed suffer from the radius of the resonant layer being far out. This, in our view, remains the most important outstanding issue for AWH. Whether or not the Kinetic Alfvén Wave can carry a large amount of energy to the centre is not yet established. Results on TCA suggest that there may be considerable core deposition.

Beta-limits. Although AWH results on TCA are extremely promising, it must be stressed that no AWH experiment has succeeded in reaching a beta-limit, which must remain the definition of a totally proven heating method.

III. AWH SPECTRUM AND LOADING FOR ASDEX UPGRADE

III.1 Introduction

To calculate the spectrum and antenna loading for ASDEX Upgrade we have used three approaches. Firstly we illustrate the spectrum using the ideal mhd dispersion relation, which is adequate for a preliminary understanding. Secondly we use a 1-D ideal mhd code which includes the terms ω/ω_{ci}, important for differentiating between resonances with $m = \pm 1$, in order to estimate the antenna loading. Thirdly we have used a 2-D ideal mhd code which does not include ω/ω_{ci} terms, to look at the effects of non-circularity, of toroidicity and of an equatorial antenna position.

In the calculations we have restricted ourselves to the following parameters :

B_T = 2.7 T
I_p = 1.6 MA
R_0 = 1.65 m
a = 0.5 m
b = 0.95 m

We have, in addition, used the three proposed density profiles [Fig. 1] namely :

(a) $n_e(0) = 2 \times 10^{14}$ cm^{-3}, $n_e(a) = 2 \times 10^{13}$ cm^{-3}, $K_n = 0.1$
(b) $n_e(0) = 8 \times 10^{13}$ cm^{-3}, $n_e(a) = 2 \times 10^{13}$ cm^{-3}, $K_n = 0.8$
(c) $n_e(0) = 2 \times 10^{14}$ cm^{-3}, $n_e(a) = 2 \times 10^{13}$ cm^{-3}, $K_n = 0.9$

where $$n_e(r) = (n_e(0) - n_e(a))\ (1 - r^2/a^2)^{K_n} + n_e(a)$$

As originally proposed to us we have assumed that 8 identical antennae will be installed in the "ICRH ports".

We have restricted ourselves in the choice of scenario to relatively low-n excitation, which has the disadvantage, as we shall see, of requiring a low frequency. It has been noted that if lateral screens prove to be essential, then they can be used to tailor the excited spectrum by cancelling the low-n modes; even further still, one could consider a modulated vessel which favours a particular n-number surface mode. We have clearly no experimental data on such a scenario from TCA. Further more, the main effect of the ω/ω_{ci} terms is to asymmetrize the excitation in the poloidal, and hence also toroidal, direction. The surface wave, even at extremely low values of ω/ω_{ci}, is not therefore a standing wave in the toroidal direction in an axisymmetric torus. A modulated torus would therefore reduce the loading of the antenna due to the net part of the surface wave which would have a travelling nature. We have not, therefore, pursued the avenue of high-n (say > 32) excitation any further.

III.2 AWH Spectrum in ASDEX Upgrade

Using the parameters of ASDEX Upgrade and <A> = 1 for a pure hydrogen discharge, equation (2) gives

$$f^2(\text{MHz}) \times n_{e_{13}}(0) = \frac{(1 + m/q(r))}{n_e(r)/n_e(0)} \times 3.24 \qquad (4)$$

The ω/ω_{ci} term has been neglected as it only slightly changes the resonance condition.

We have plotted this relationship for the three reference profiles in Figs 2-4 using a simple equivalent cylindrical q-profile, adequate for the moment, given by $j(r) = j(0)\ (1 - r^2/a^2)^{K_j}$; $K_j = (q(a)/q(0) - 1)$ and $q(a) \sim 2.4$, $q(0) = 0.95$.

We make the following observations from these figures :

a) The combination of a very flat density profile and a fairly flat q-profile typified by the case (a) leads to a flat $f^2 \cdot n_e(0)$ profile which puts the resonant surfaces close to the plasma edge, much more quickly than in case (c).

b) The assumption of a large relative pedestal in case (b) compared with case (c) also leads to a flatter $f^2 \cdot n_e(0)$ profile.

c) The resonant surfaces are fairly well grouped according to their $|n+m|$ value, for the assumed case of small radial variation in q.

d) We see that as $f^2 \cdot n_e(0)$ increases, the number of possible resonant surfaces increases, most of which lie at the edge. We have, in addition, only shown $m=0,\pm1$ resonant surfaces which probably account for most of the antenna loading.

e) We have marked the frequency corresponding to the actual peak density chosen in each case. It should be remembered that only the shape of the density profile defines the form of these curves. We see clearly that a change of frequency or mode is required to track a particular resonant surface as the central density changes by the given factor of 2.5.

f) The flat $f^2 \cdot n_e(0)$ profile of case (a) does not even allow mode-changing to retain the surface in the plasma.

What is therefore a correct scenario for low-n AWH ? Unfortunately, we must make an assumption concerning the power deposition which is not yet experimentally determined. We assume that it is important to retain a reasonably central resonant layer ($r < 2a/3$) in order to heat efficiently. It must be noted (parenthetically) that the evidence for this on TCA is by no means clear. It remains however an extremely stringent assumption.

In Figure 5 we show the evolution of the surface configuration at a frequency of 4.47 MHz from a starting density of 2.5×10^{13} cm^{-3} to a final density of 2×10^{14} cm^{-3}, using the profile shape given in case (c). We see that a change of mode is required at 8×10^{13} cm^{-3}, from N=4 to N=8, simply accomplished by a phase inversion of every second antenna. An intermediate N=6 configuration using each second antenna would inevitably excite n=2 surfaces right at the edge of the plasma. Similarly the use of running waves defined by antenna phasings will also lead to n-number ambiguity.

In Figure 6 we show the same scenario as Figure 5, but following the evolution of a case (a) density profile. We see there is now actually a region where the resonance layer is only at the plasma edge. In this case we are slightly better off with a lower-n excitation, alternating between N = 2 and N = 4, as shown in Figure 7(a), but at half the frequency, namely 2.23 MHz. There is not such a large gap, but the surfaces are less favourably further out. Figure 7(b) considers N=1,2 and 4 excitation at the same frequency for a case (c) profile. This will be discussed further in section IV.

It is clear that an antenna circuit which can be driven efficiently at two separate frequencies using N = 4 and 8 provides a better means of avoiding this problem. A jump by a factor of 2 in f^2 to fill in the gap in Fig. 6 would be useful, i.e. 4.47 MHz and 6.32 MHz. It is clear that this would introduce an extra complexity in the antenna tuning circuit. We cannot, finally, predict the behaviour of AWH in a case with such a flat density profile; such profiles are not produced in TCA.

We see now that ω/ω_{ci} for these scenarios lies between 0.05 -

0.16. Equation (4) is not, therefore, changed by much when including the terms in ω/ω_{ci}.

III.3 Antenna Loading - Cylindrical calculation

We have calculated the loading as a function of generator frequency for the two reasonable cases of density profiles, using a cylindrical code including terms ω/ω_{ci} [9] and assuming an equivalent value of q(a) = 3.3. The finite toroidal and poloidal widths of the antenna are correctly taken into consideration, and the Fourier components m = ±1 are calculated. We neglect the direct loading due to m = 0, m = ±2, etc... which are seen on TCA to be relatively small. The main problem encountered in this model is the return current in the antenna, not explicitly described in the code but assumed to be on the conducting shell. We have calculated therefore a cylindrical plasma of minor radius $\langle a \rangle \sim \sqrt{ab} = 0.65$ m in a vessel where the wall is at a) $r_w=1.25 \langle a \rangle$ and b) $r_w=1.45 \langle a \rangle$. The active antenna element is considered to be at $r_{ant}=1.15 \langle a \rangle$. The first case gives a severe under-estimate of the antenna loading and the second case will be an overestimate. The difference of roughly a factor of two illustrates the requirement for a large toroidal flux-area antenna in AWH. This would lead to an increased antenna voltage for a given rf current, compensated by improved loading and an improved ratio between antenna losses and anenna loading. In Figure 8 we sketch an antenna which should couple better for AWH, while remaining inside the proposed ICRH Faraday Shield. In Figure 9(a,b) we show the loading curves for N = 4 and N = 8 as a function of generator frequency calculated for the case $r_w=1.45 \langle a \rangle$.

We must not forget that the 1-D model does not include the toroidal coupling to the m=0 resonance which increases the loading where it is small in a 1-D calculation - i.e. below the first directly excited DAWs. The usable range of a particular toroidal mode number is therefore increased.

To conclude the 1-D calculation, we note that the total antenna loading is in the range 0.25 to 1.4 Ω in the useful range of excitation. In what follows we have taken 0.4 Ω as being a pessimistic typical value.

III.4 Resonance Structure - 2-D calculations

Important restrictions of the 2-D numerical model [10] are its assumption of up-down symmetry, its representation of the antenna as an infinitely thin shell enclosing the plasma and the large uncertainty in the value of the antenna loading. As with the one-dimensional model dissipation is artificially introduced and assumed local to the resonance layers.

With the above constraints in mind we have considered the lower section of typical ASDEX Upgrade equilibrium and approximated a double-null divertor. This should provide a "worst-case" for edge coupling. The main parameters of this equilibrium are given in Fig. 10 along with the vacuum chamber, antenna surface and plasma geometry. The calculations have concentrated on density profile (b) as this has a reasonable set of resonance layers that can be excited at a given frequency. The antenna current distribution is reduced smoothly from the feeds to give all the current on the low-field side. Unfortunately the discretisation has not been optimised so the results must be regarded as preliminary. This is most critical for the absolute value of antenna loading but is much less important for estimating at which resonance layer the energy is converted.

In Fig. 11 we present the results for N=4 excitation at (a) 2.5 MHz and (b) 3.1 MHz. At the former the m=0 layer is at r/a ~.3 while at the latter the m=1 layer has appeared and is at r/a ~.45. Obviously a large portion of the energy is converted at the edge. The appearance of the m=1 layer not only increases the antenna loading by a factor of 2 but also reduces edge losses due to the good coupling of the antenna to the n=4, m=1 compressional wave (see Fig. 9(a)).

It should be noted that our previous studies have indicated that low-field excitation is particularly hampered by coupling to edge modes. For comparison in Fig. 11(b) we show the results of high-field side excitation using the inner-wall protection shield as an antenna. It appears that the low-field/high-field difference is much less marked for an elliptical rather than circular plasma. Flatter density

profiles (profile (a)) also alleviate the problem by providing a reduced set of resonance layers at a particular frequency.

IV. TOROIDALLY ASYMMETRIC ANTENNAE - SPECTRUM EXCITED

IV.1 Excited spectrum

The present plan (Spring 85) on ASDEX Upgrade is to have 4 ICRH launchers instead of the 8 previously assumed, and to position them asymmetically toroidally, i.e. at toroidal angles $\phi = 0, \pi/2, \pi, -\pi/4$. This introduces a degree of uncertainty but also flexibility, and we study its implications in this section.

If we write the antenna structure as a sum of cylindrical Fourier components:

$$j_\phi(\theta,\phi) = \sum_{n,m} A_{nm}\, e^{i(n\phi+m\theta)}$$

then

$$A_{nm} = \frac{1}{4\pi^2} \iint j_\theta(\theta,\phi) e^{-i(n\phi+m\theta)} d\theta d\phi$$

For 8 symmetric antennae this becomes

$$A_{nm} = \frac{2I}{\pi^2 \phi_A R} \cdot \frac{\sin m\theta_A}{m} \cdot \frac{\sin n\theta_A}{n} \times \begin{cases} 2 & \text{(n-even)} \\ \sqrt{2} & \text{(n-odd)} \end{cases}$$

where the antenna poloidal subtended angle is $2\theta_A$ and the toroidal subtended angle is $2\phi_A$. If the antennae are not symmetric we must calculate the full component strengths A_{nm} summing over all the active antennae whose currents are C_j and phases Ψ_j. With only four antennae to excite, we only consider n = 1-4. In order to perform an analysis of the antenna structures we assume that each resonant surface with m = ±1 has unit loading and we neglect, therefore, all considerations of toroidal coupling and differences between the modes with different n.

It is instructive to consider the aim of the exercise as depositing the maximum power or maximum fraction of the power into a particular n-number. With the simplification outlined, the power deposited in each n-number becomes :

$$P_n \sim A^2_{n1}$$

We can therefore maximise P_n or optimise $R_n = P_n/\Sigma P_n'$ for the different n.

(a) n = 1. This is the trivial case in which (see Fig. 4) no other n's are assumed to be resonant, or at least contributing to the deposited power. R_n is therefore 100% for any combination of currents and phases. C_j = 1,-1,-1,1 and Ψ_j = 0,0,0,0, giving an optimal value of Q_1 = 10.2, where $Q_n = P_n/\text{Max}(C_j)^2$.

(b) n = 2. We can optimise this case analytically yielding R_2 = 95%, depositing 5% in the n=1 layers. We obtain C_j = 1,-1,1,-.71, Ψ_j = 0,0,0,0 and Q_2 = 9.5. We can increase Q_2 to 10.0 by changing C_j to 1,-1,1,-1 but R_2 then becomes 94.4%. Such a choice would clearly be made experimentally.

(c) n = 3. This is the poorest of the four cases, since the antenna structure has no real n=3 symmetry inherent in it. We obtain, by trial and error optimisation, an optimal R_3 = 57% with C_j = 1,1,1,1 and Ψ_j = 0,0,0,0. This structure only has Q_3 = 3.4 and would therefore be less interesting. If we alter the phasings to C_j = 1,1,-1,-1 and Ψ_j = 0,0,0,0 we obtain Q_3 = 7.4, i.e. over double the power for the same maximum antenna current, but R_3 has reduced to 53%. 33% of the power now goes into the n=1 layers. Whether or not n = 3 would be a useful addition to the excited spectra would be experimentally determined.

(d) n = 4. The simplest phasing structure, namely C_j = 1,1,1,-1 and Ψ_j = 0,0,0,0 leads to R_4 = 73% (15% into n = ±1) and Q_4 = 16, clearly the maximum possible for four antennae. We can increase the spectral purity to R_4 = 75% using C_j = 1,1,1,-0.707, Ψ_j = 0,0,0,0

giving a reduced Q_4 = 13.7 (13.7% in n = 1). We can reduce the fraction into n = 1 to 8.3%, retaining R_4 = 75% but again reducing Q_4 to 9 by phasing C_j = 1,1,1,0, Ψ_j = 0,0,0,0, i.e. by using only 3 antennae !

We conclude (i) that n = 1,2,4 can be efficiently excited using asymmetric antennae, with the worst case being 25% into the lower-n resonant layers, and (ii) that n = 3 might possibly be a useful addition to the spectrum depending on the physics imponderables. A summary of the useful phasings is given in Table I. Figure 7b) shows a 2.23 MHz density ramp using N = 1,2 and 4 for a case (c) density profile.

In the optimisation described we have, for simplicity, not differentiated between ±n. The system of antennae described can excite a travelling wave structure for n = ±1,±2,±3 by correct phasing. Since it has been shown experimentally and theoretically that m = -1 absorbs more power than m = +1 in TCA conditions, the choice of ±n also defines the helicity n/m. This fact can therefore be used to preferentially excite one or other of the two resonant surfaces with the same n, split by the q-profile. This would undoubtedly lead to a more advantageous heating scenario, but we have not followed this further.

Table I Summary of useful phasings.

n	C_j	Ψ_j	Q_n	R_n
1	1 -1 -1 1	0 0 0 0	10.2	100%
2	1 -1 1 -.707	0 0 0 0	9.5	95%
3	1 1 1 1	0 0 0 0	3.4	57%
	1 1 -1 -1	0 0 0 0	7.4	53%
4	1 1 1 -1	0 0 0 0	16.0	73%
	1 1 1 -.707	0 0 0 0	13.7	75%

IV.2 Loading curves

We have calculated the loading curves for the optimal cases found

in the previous sub-section and they are shown in Figure 12(a-d), for which we have taken the density profiles (c) of Figure 1, H_2, and a frequency of 2.5 MHz. The contributions for n = ±1,±2,±3,±4 have been calculated, using the same method as described in Section III.3. In addition, out of interest, we have calculated one case for density profile (b), and this is shown in Figure 12(f). The x-axis is

$$\omega^* = f(\text{MHz}) \sqrt{n_{e_{13}}(0)}$$

Figure 12(a) shows considerable loading at $\omega^* \sim 2\text{-}4$ corresponding to the n=±1 continua. Figure 12(b) shows the step at $\omega^* \sim 5$ corresponding to the (n,m)=(2,1) continuum threshold. Figure 12(c) similarly shows an increase at $\omega^* \sim 7$ corresponding to the target resonance (n,m)=(3,1), but in this case we see that there is a substantial loading at much lower values of ω^*, corresponding to the spectral impurity foreseen in the preceeding sub-section. Figure 12(d) shows a very pure case with a large increase at the (n,m)=(4,1) threshold at $\omega^* \sim 9$. Figure 12(e) corresponds to the 3-antenna case to be compared with the 4-antenna case. We see in Figure 12(f) that a substantial loading is also obtained for the flatter profile (b).

V. ANTENNA CIRCUIT

We limit ourselves to a single turn antenna. A multi-turn antenna will reduce the antenna feed current by the number of turns, and will increase the feed voltage by the number of turns, for a given power. Nonetheless we feel that to assume a multiple-turn antenna would be an error, since the current capability of the feed is not yet proven to be prohibitive. The risk of shorting between turns is not easily assessible, even with a Faraday Shield. The concept remains nonetheless an interesting one which TCA might find time to test in the future.

We also restrict ourselves to the circuit design used on TCA, namely a tuned circuit as close as possible to the antennae, with a low impedance transmission line between the lumped capacitance and the

antenna. On TCA we use 18x50 Ω cables to each antenna terminal giving a 5 m 5.6 Ω line. The losses in the tuned circuit are relatively high (60-100 mΩ per antenna) and should be lower for ASDEX Upgrade. There is no problem in constructing such a line, even with reduced physical access. The matching capacitor box, of the order of 0.5 m^3 per antenna group for TCA will not obstruct any access since its positioning is not critical relative to the antennae. The tuned-circuit losses evidently increase with increasing distance from the antenna. At a major radius of 5.0 m, 2.5 m from the antenna feed, the losses will be tolerable.

Each antenna tuned circuit will be fed in push-pull from a separate fixed-frequency generator with remote phase-control, much simpler than the AFCO tunable generator constructed for TCA [8]. The antenna circuit can be floating with respect to the torus, as in TCA. These units can be at a certain distance from their tuned-circuits (at least 4 m), avoiding conflicts with diagnostic access requirements.

The lack of specific design in this section reflects the simplicity of such a low-frequency high current system using conventional technology. The details can be adjusted to fit around other design constraints. No problems in designing a reasonably loss-less system are foreseen given the geographical constraints mentioned. A sketch of the antenna circuit is shown in Fig. 13.

VI. GENERATOR REQUIREMENT

The preceeding arguments suggest an rf antenna current of several kA at a frequency of 2-4 MHz. The power delivered to the plasma is given by

$$P = \frac{1}{2} \hat{I}^2_{ant} R_{ant}; \quad \hat{I}(kA) = 2.23 \sqrt{P(MW)} \quad (R_{ant}=0.4\ \Omega)$$

Thus to deliver a typical value of 4 MW we need I ~4.5 kA. Since the antenna loading is small (~30-200 mΩ per antenna) the losses in the ringing circuit must be kept small, as mentioned.

The existing available DC power sources, namely units of 3.08 MW [22 kV • 140 A] could be conveniently used to power the AWH units. We do not consider that the planned ICRH generator could be usefully adapted to work at our proposed low frequency as a regular extension to its ICRH operating range (80-120 MHz). Nonetheless the DC supply represents a considerable available investment. The tubes required for ICRH are more expensive than the industrial heating triodes used on TCA. They could however be used, with their heating supplies and control, at the lower frequency although considerable rebuilding would be necessary.

The total system efficiency from DC supply output to the antenna loading power is estimated to be of the order of 25% for a non-tunable system. A detailed cost estimate has not been prepared, but the system is much simpler than the AFCO system. An approximate cost estimate from the DC supply output to the antenna feed, using no existing equipment, is 2 Sfr/Watt delivered.

VII. IMPLICATIONS FOR ASDEX UPGRADE

The low-n AWH scenario developed implies a low excitation frequency. This, in turn, implies a low antenna loading compensated by a high antenna current. The high oscillating current does not, in general, lead to a large antenna voltage since

$$V \sim \omega LI \sim \omega L\sqrt{P}/R_{ant}$$

and R_{ant}, the antenna loading, does not decrease as fast as ω^2.

Two fundamental requirements exist, therefore, if we are to use the ICRH antennae for AWH :

a) Capability of feeding the antenna with a larger current, but at lower voltage. Since the ICRH feed has not yet been designed for ASDEX Upgrade, we assume that the design could be rendered capable of feeding a greater current.

b) Reduction of the resistive losses in the antenna itself, both the conductors and the Faraday Shields. Internal conductors are to be

coated in silver, and the thickness of the coating must be increased by a factor of $\sqrt{f_{ICRH}/f_{AWH}}$ in order to retain a couple of skin-depths. This ratio is $\sim\sqrt{30/2.23} = 3.7$ taking the lower AWH frequency discussed. We estimate that 60 μm of silver would be adequate. The design of the ICRH Faraday shields calls for 6 μm of TiC CVD-deposited on 20 μm of copper galvanically coated onto stainless steel. We would need to increase the thickness of the 20 μm copper layer to 65 μm, again to have two skin-depths of copper. In this way almost all the rf losses occur in the copper layer.

It is clear, however, that even when allowing for two skin-depths, the antenna losses will increase as the frequency is lowered since

$$\frac{P_{loss}}{P_{load}} \sim \frac{\sqrt{\omega}}{\omega} \sim \frac{1}{\sqrt{\omega}}$$

We estimate the ratio P_{loss}/P_{load} in each antenna to be

$$\frac{l\rho/2\omega\delta}{R_{ant}} \sim \frac{1.4m\Omega}{50m\Omega} \sim 3\% \qquad \text{(assuming Cu).}$$

It is thus clear that a wider antenna than the proposed ICRH antenna would suit low-n AWH better since firstly the antenna inductance will be reduced, further reducing the antenna voltage, and secondly the antenna resistance will be reduced relative to the antenna loading. In addition an antenna linking more toroidal flux would also be advantageous (Fig. 8).

VIII. CONCLUSIONS

The number of available antenna ports (4 or 8) would make ASDEX Upgrade a very suitable machine for low-n Alfvén Wave Heating.

The limited poloidal access (equatorial outside antennae) is not particularly disadvantageous in terms of excitation of "unwanted" modes via toroidal coupling. Mode-control would be essential to

cover the suggested density range at fixed frequency, but only entails control of the sign of the antenna current.

The antenna loading, for all antennae, is estimated to be of the order of 0.4 Ω, leading to a favourable ratio of antenna resistive loss to antenna loading.

The ICRH antenna is too narrow for operation at minimum voltage. The return current conductor is also too close to the active current conductor for AWH. An antenna specifically designed for AWH would need to modify both of these parameters.

The ICRH antennae planned for ASDEX Upgrade could be used for pilot AWH studies, even at high power, provided the current capability of the feeds is increased.

Considerable use might be made of existing equipment for the AWH generator which is technically much simpler than a higher frequency generator.

ACKNOWLEDGEMENTS

We acknowledge useful discussions with many members of the CRPP especially A. Lietti, and with Dr. J. Neuhauser of IPP-Garching who injected several new ideas. The work was partly supported by the Swiss National Scientific Research Foundation.

REFERENCES

[1] G.A. Collins et al., Lausanne report LRP 256/85

[2] A. de Chambrier et al., Plasma Phys. 24, 898 (1982)

[3] A. de Chambrier et al., Plasma Phys. 25, 1021 (1983)

[4] R. Behn et al., Plasma Physics 26, 173 (1984)

[5] A. de Chambier et al., IAEA Conference (London), Vol. 1, 531 (1984)

[6] G.A. Collins et al., EPS Conference (Budapest), Vol. 2, 248 (1985)

A. de Chambrier et al., EPS Conference (Budapest), Vol. 2, 264 (1985)

[8] A. Lietti and G. Besson, Lausanne report LRP 264/85, accepted for publication in J. Phys. E.

[9] K. Appert and J. Vaclavik, Plasma Phys. 25, 551 (1983)

[10] K. Appert et al., Nucl. Fusion 22, 903 (1982)

FIGURE CAPTIONS

1. Asdex-Upgrade reference profiles.
2. Dispersion curves for profile "a".
3. Dispersion curves for profile "b".
4. Dispersion curves for profile "c".
5. Density ramp using N=4 + N=8, profile "c", 4.47 MHz.
6. Density ramp using N=4 + N=8, profile "a", 4.47 MHz.

7a) Density ramp using N=2 + N=4, profile "a", 2.23 MHz.

b) Density ramp using N=1, N=2 + N=4, profile "c", 2.23 MHz.

8. Improved flux-linkage for AWH.

9a) 1-D calculated loading curve, N=4, profiles "b", "c".

b) 1-D calculated loading curve, N=8, profiles "b", "c".

10. 2-D calculation: input parameters.
11. 2-D energy flux for 2.5 MHz and 3.1 MHz with both LFS and HFS excitation, n=4.
12 1-D calculated loading curves for the case of a non-periodic excitation structure, 2.5 MHz.
13. Schematic of the antenna circuit.

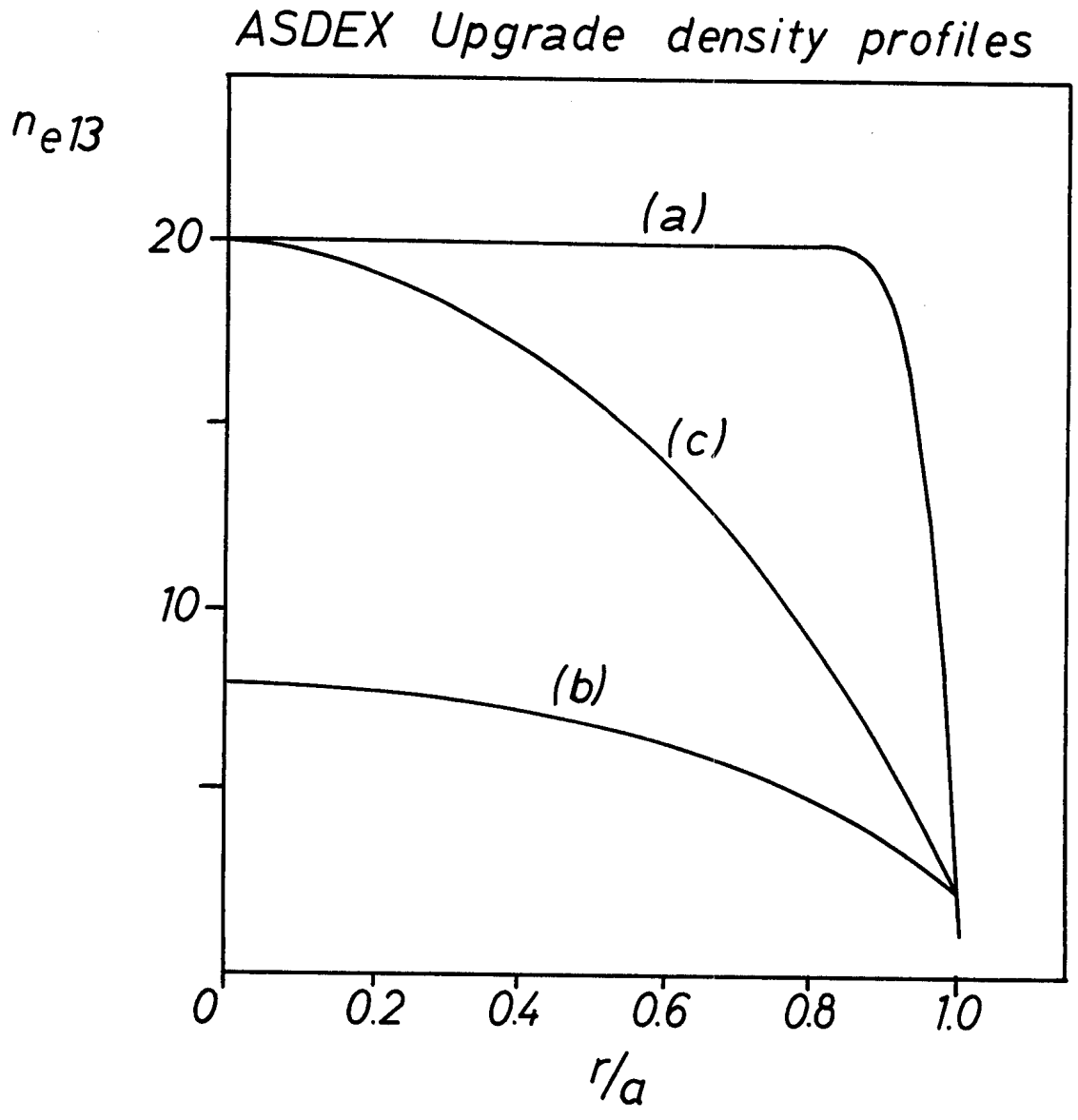
ASDEX Upgrade density profiles
n_{e13}
20
10
0
0.2
0.4
0.6
0.8
1.0
r/a
(a)
(b)
(c)

Figure 1

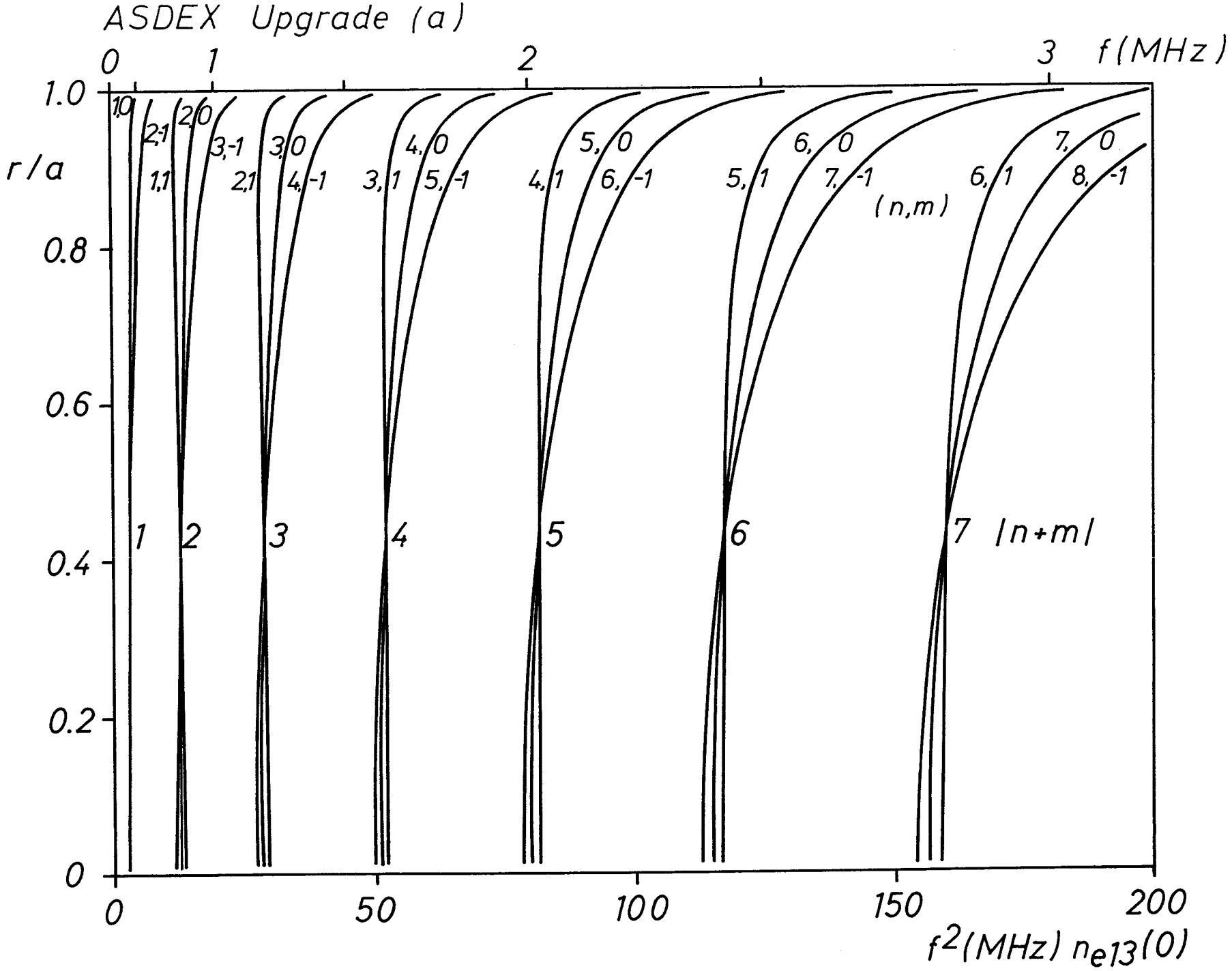
ASDEX Upgrade (a)
0
1
2
3
f(MHz)
1.0
r/a
0.8
0.6
0.4
0.2
0
1,0
2,-1
1,1
2,0
3,-1
2,1
3,0
4,-1
3,1
4,0
5,-1
4,1
5,0
6,-1
5,1
6,0
7,-1
(n,m)
6,1
7,0
8,-1
1
2
3
4
5
6
7
|n+m|
0
50
100
150
200
f²(MHz) ne13(0)

Figure 2

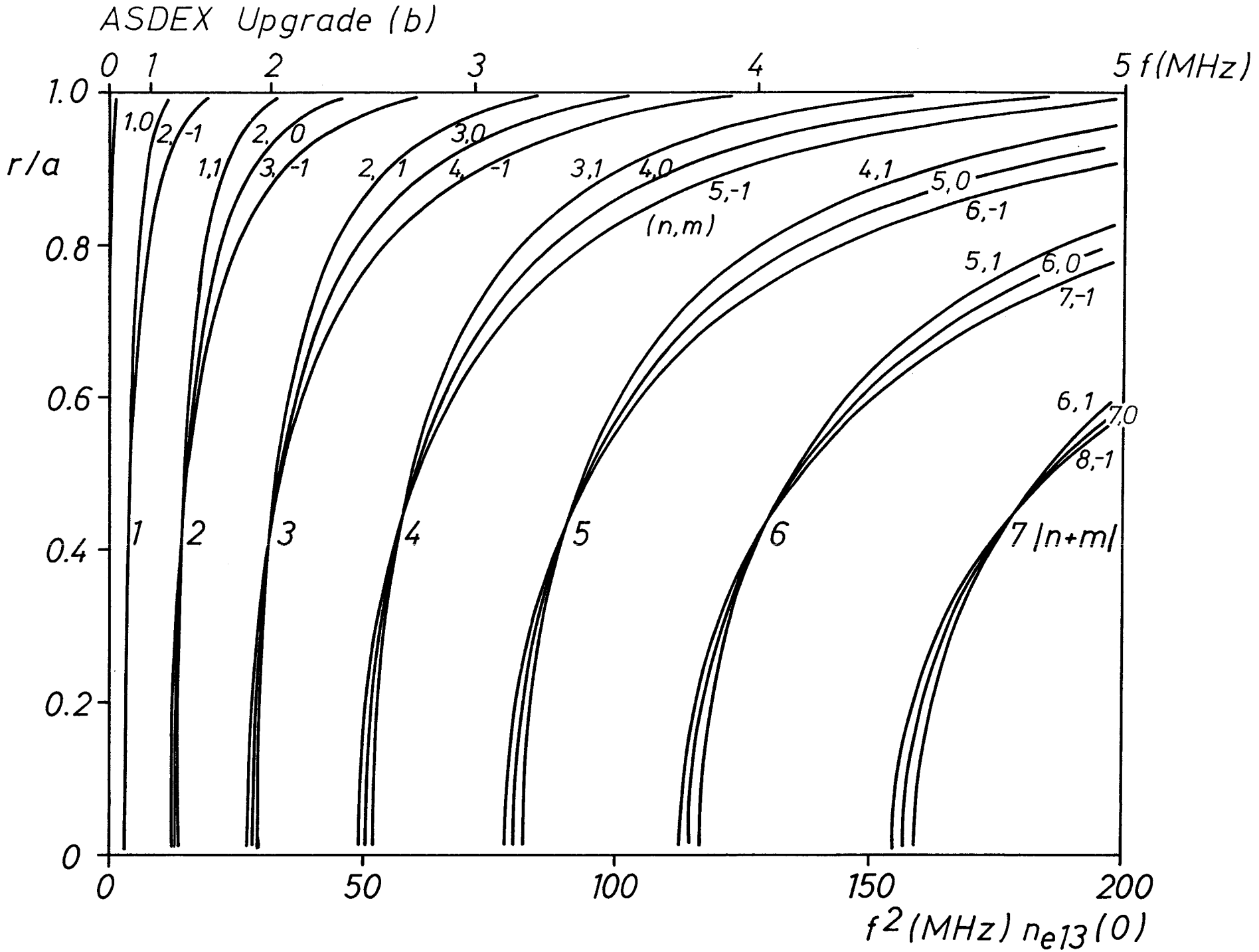
ASDEX Upgrade (b)
0
1
2
3
4
5 f(MHz)
1.0
r/a
0.8
0.6
0.4
0.2
0
1,0
2,-1
1,1
2,0
3,-1
2,1
3,0
4,-1
3,1
4,0
5,-1
4,1
5,0
6,-1
5,1
6,0
7,-1
6,1
7,0
8,-1
(n,m)
1
2
3
4
5
6
7 |n+m|
0
50
100
150
200
f² (MHz) n_e13 (0)

Figure 3

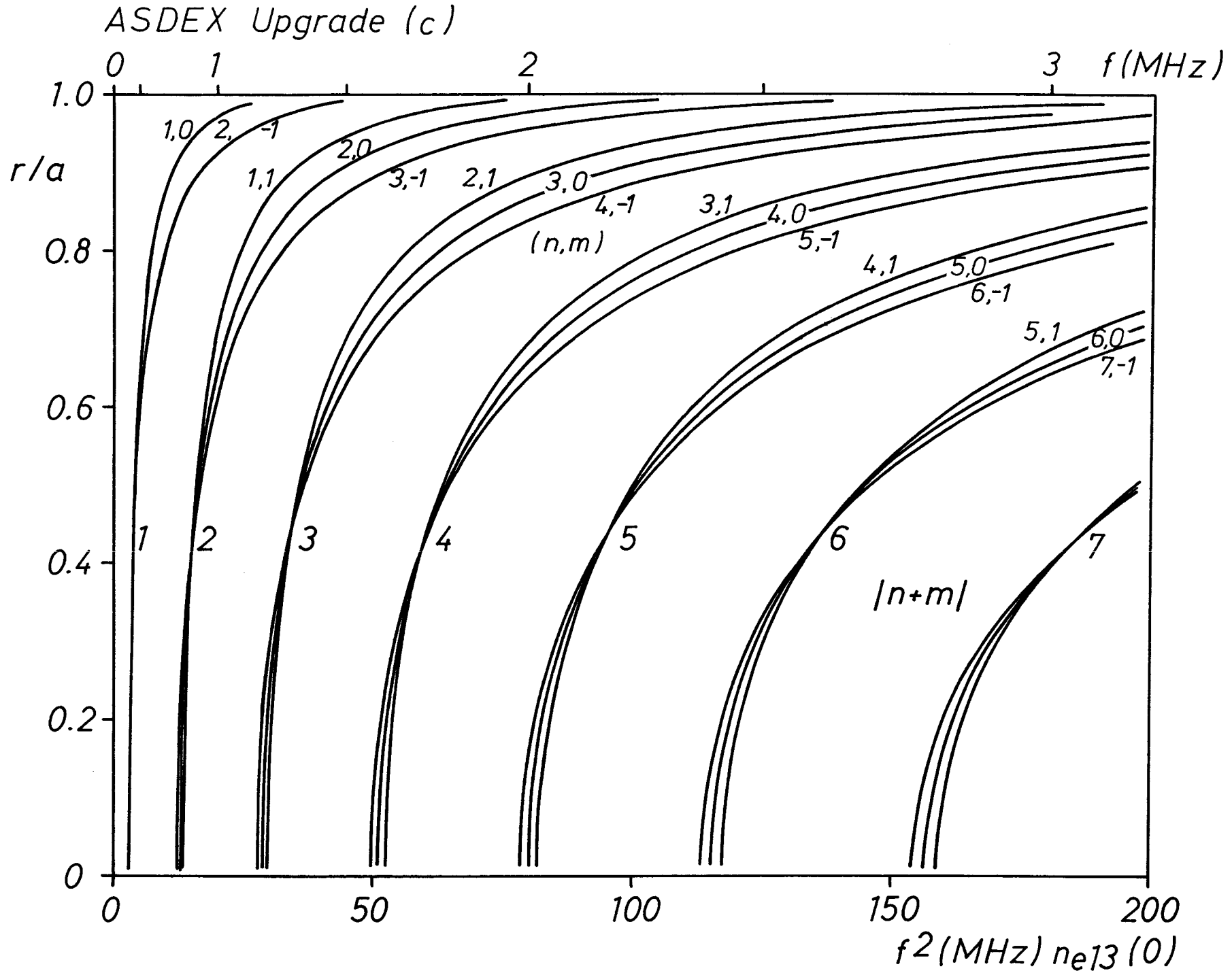
ASDEX Upgrade (c)
0
1
2
3
f(MHz)
1.0
r/a
0.8
0.6
0.4
0.2
0
1,0
2,-1
2,0
1,1
3,-1
2,1
3,0
4,-1
3,1
4,0
5,-1
(n,m)
4,1
5,0
6,-1
5,1
6,0
7,-1
1
2
3
4
5
6
7
|n+m|
0
50
100
150
200
f²(MHz) ne13(0)

Figure 4

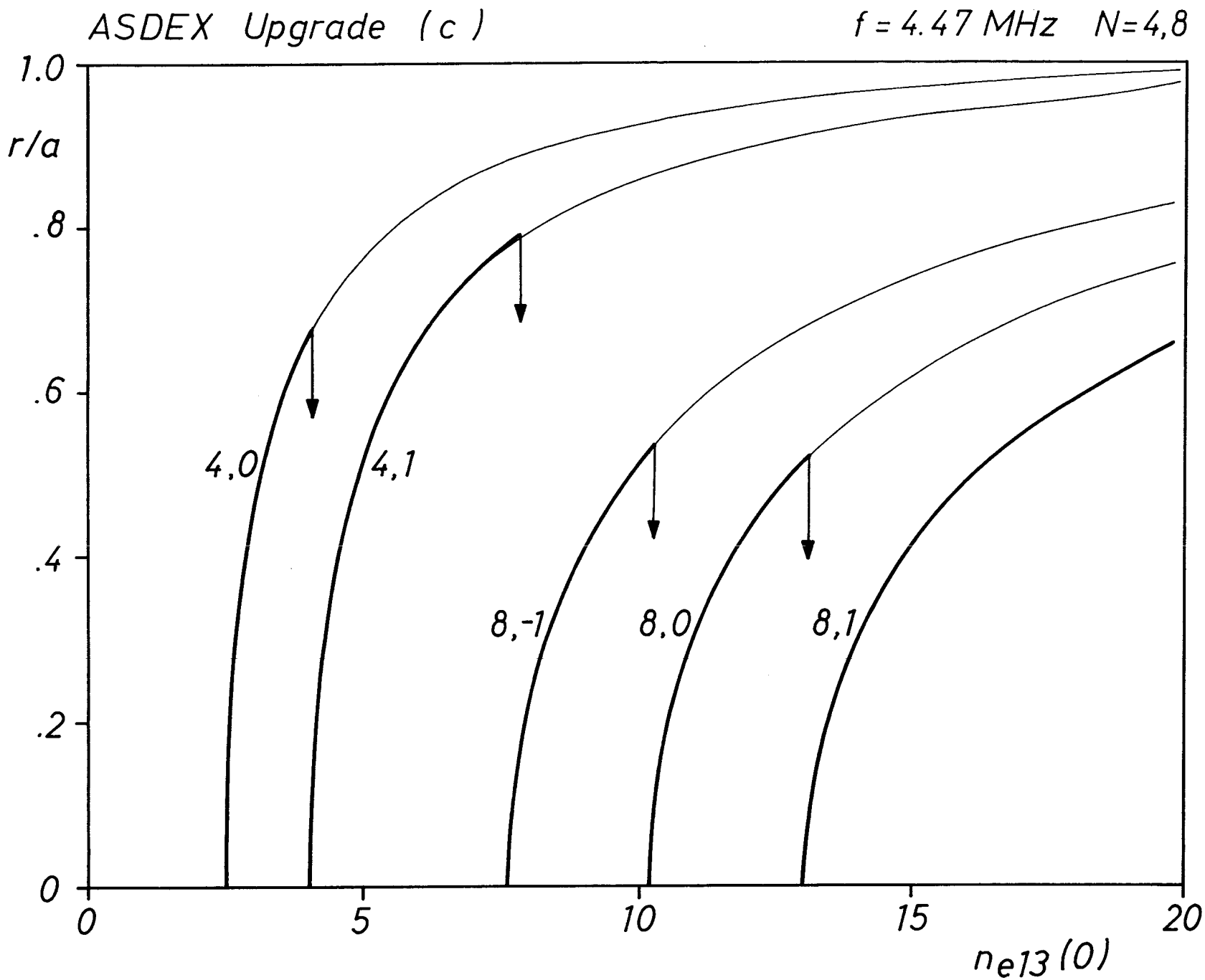
ASDEX Upgrade (c)
f = 4.47 MHz N=4,8
1.0
r/a
.8
.6
.4
.2
0
4,0
4,1
8,-1
8,0
8,1
0
5
10
15
20
ne13 (0)

Figure 5

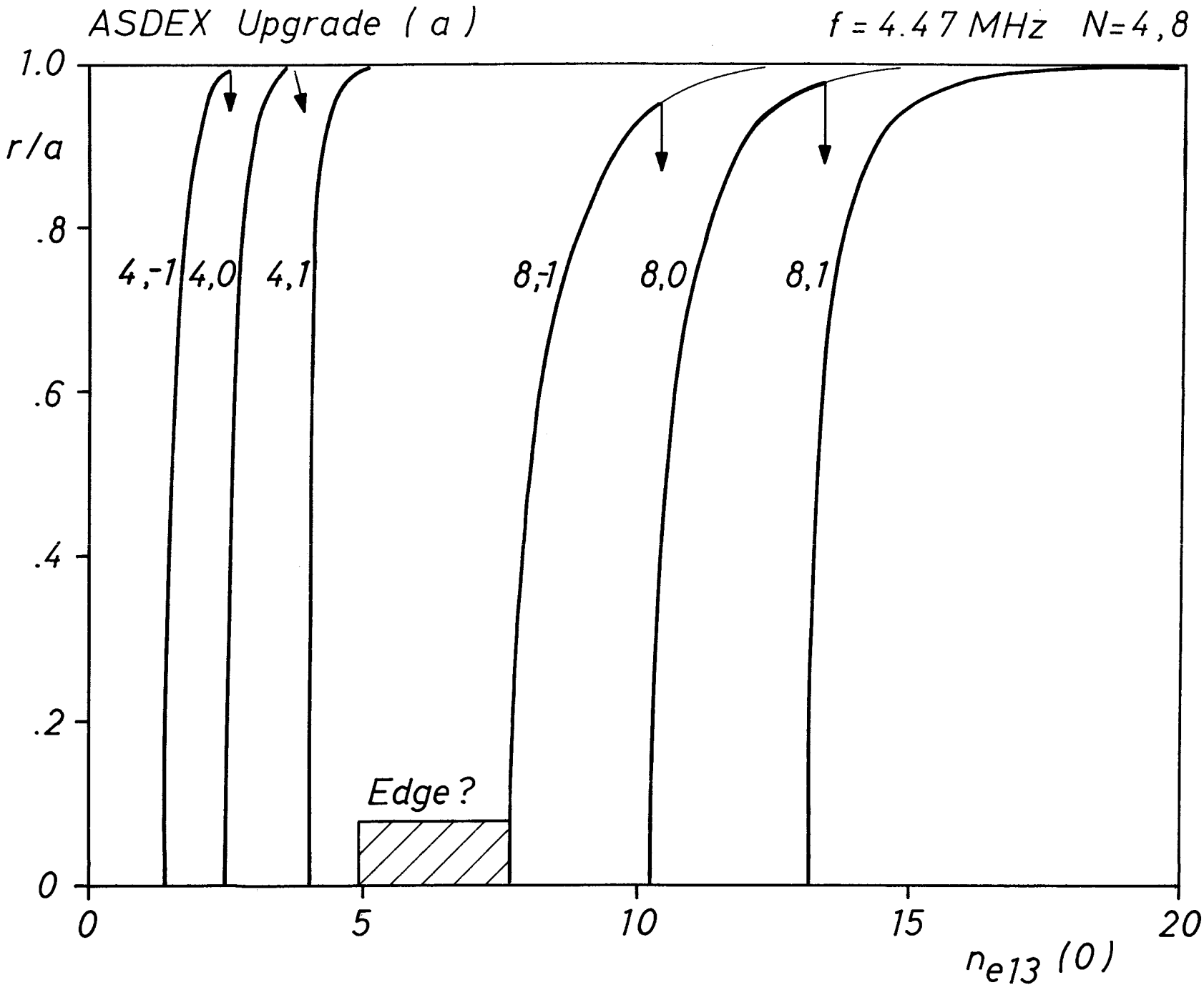
ASDEX Upgrade (a)
f = 4.47 MHz N=4,8
1.0
r/a
.8
.6
.4
.2
0
4,-1
4,0
4,1
8,-1
8,0
8,1
Edge?
0
5
10
15
20
n_{e13} (0)

Figure 6

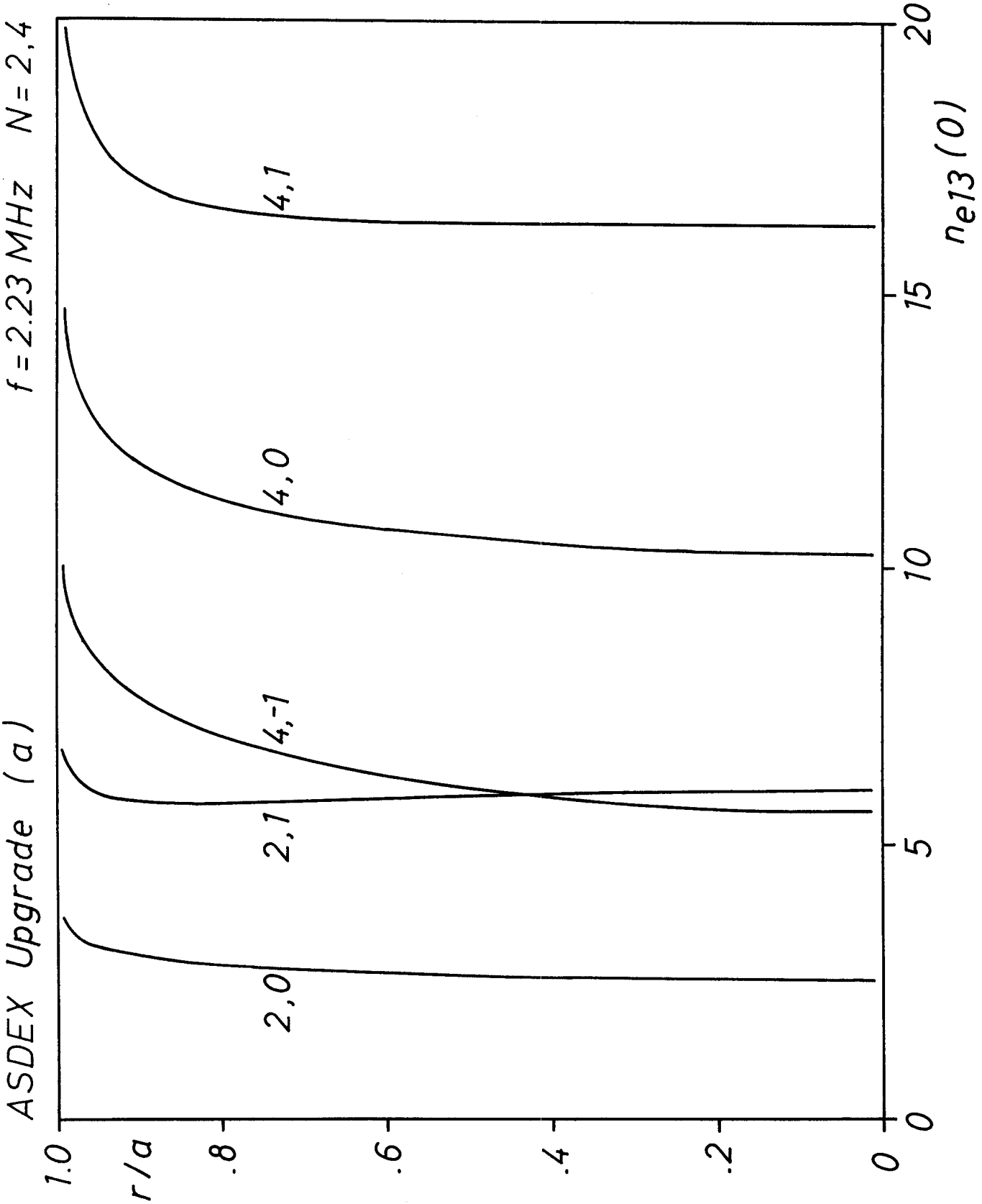
ASDEX Upgrade (a)
f = 2.23 MHz N = 2,4
r/a
1.0
.8
.6
.4
.2
0
0
5
10
15
20
$n_{e13}(0)$
4,1
4,0
4,-1
2,1
2,0

Figure 7(a)

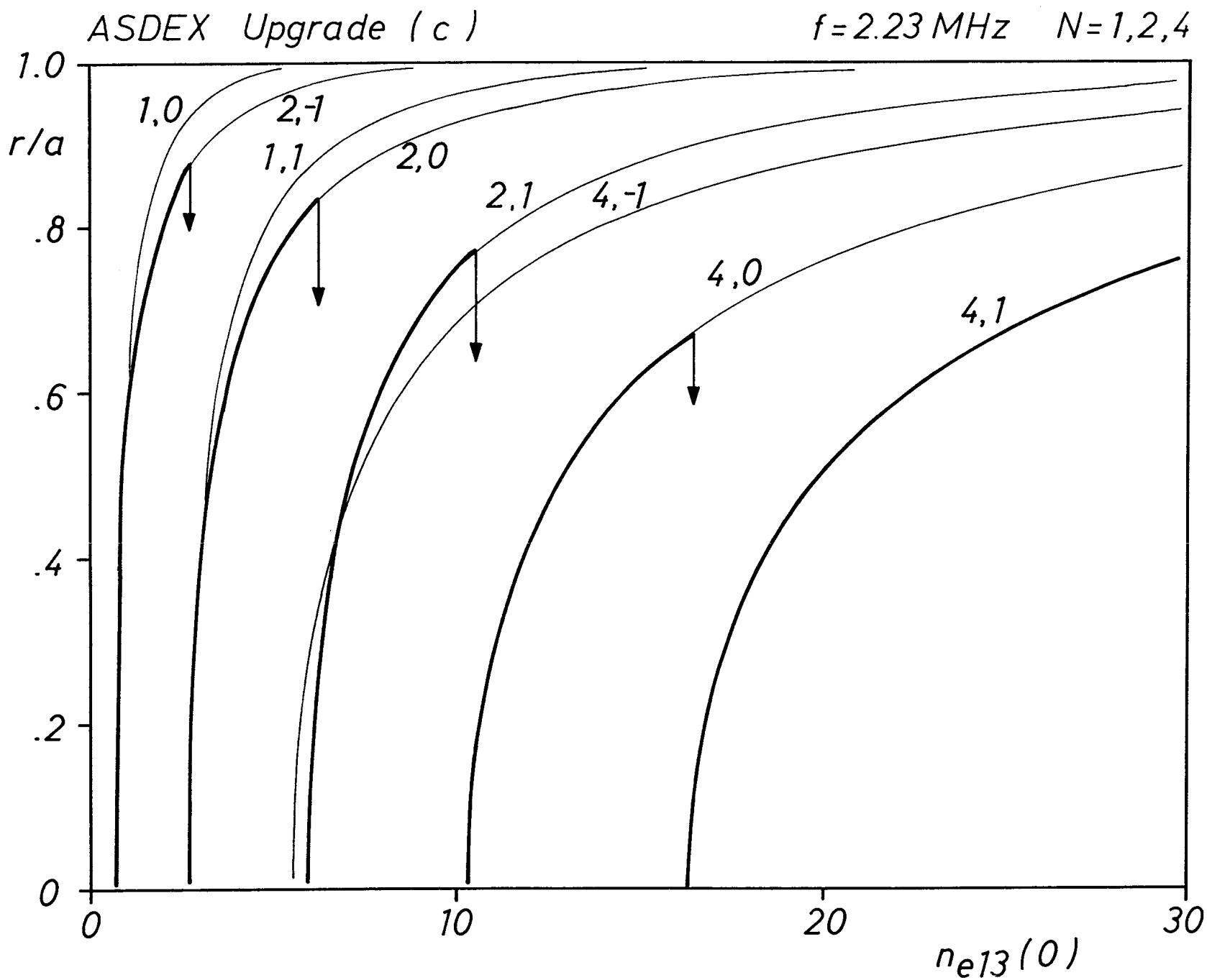
ASDEX Upgrade (c)
f = 2.23 MHz N = 1,2,4
1.0
r/a
.8
.6
.4
.2
0
1,0
2,-1
1,1
2,0
2,1
4,-1
4,0
4,1
0
10
20
30
$n_{e13}(0)$

Figure 7(b)

ASDEX Upgrade
Antenna modification

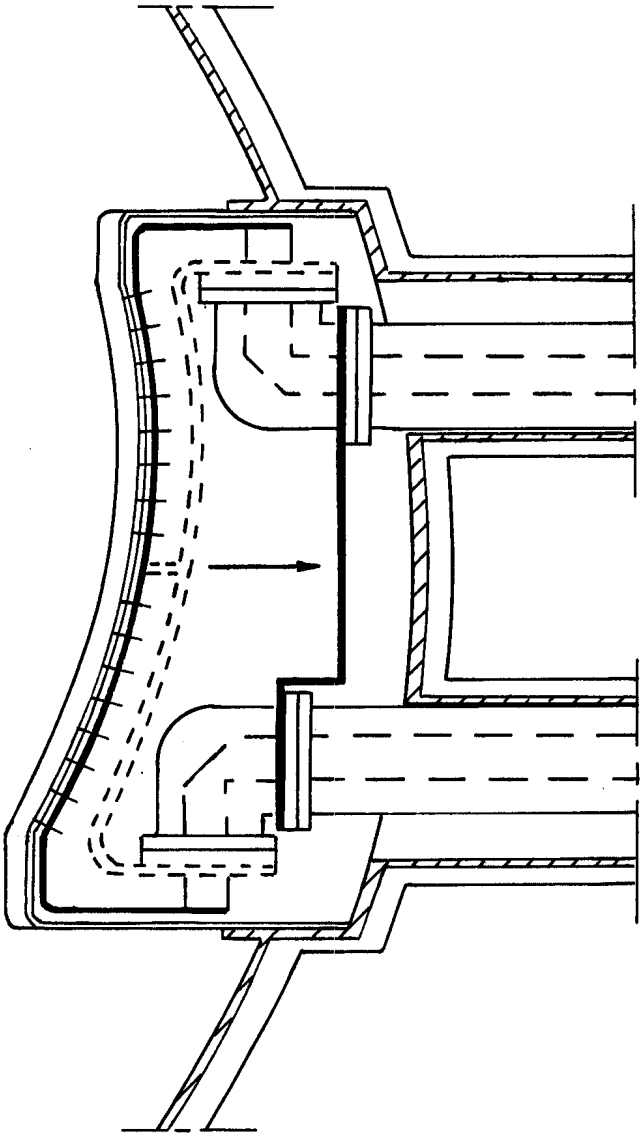

Figure 8

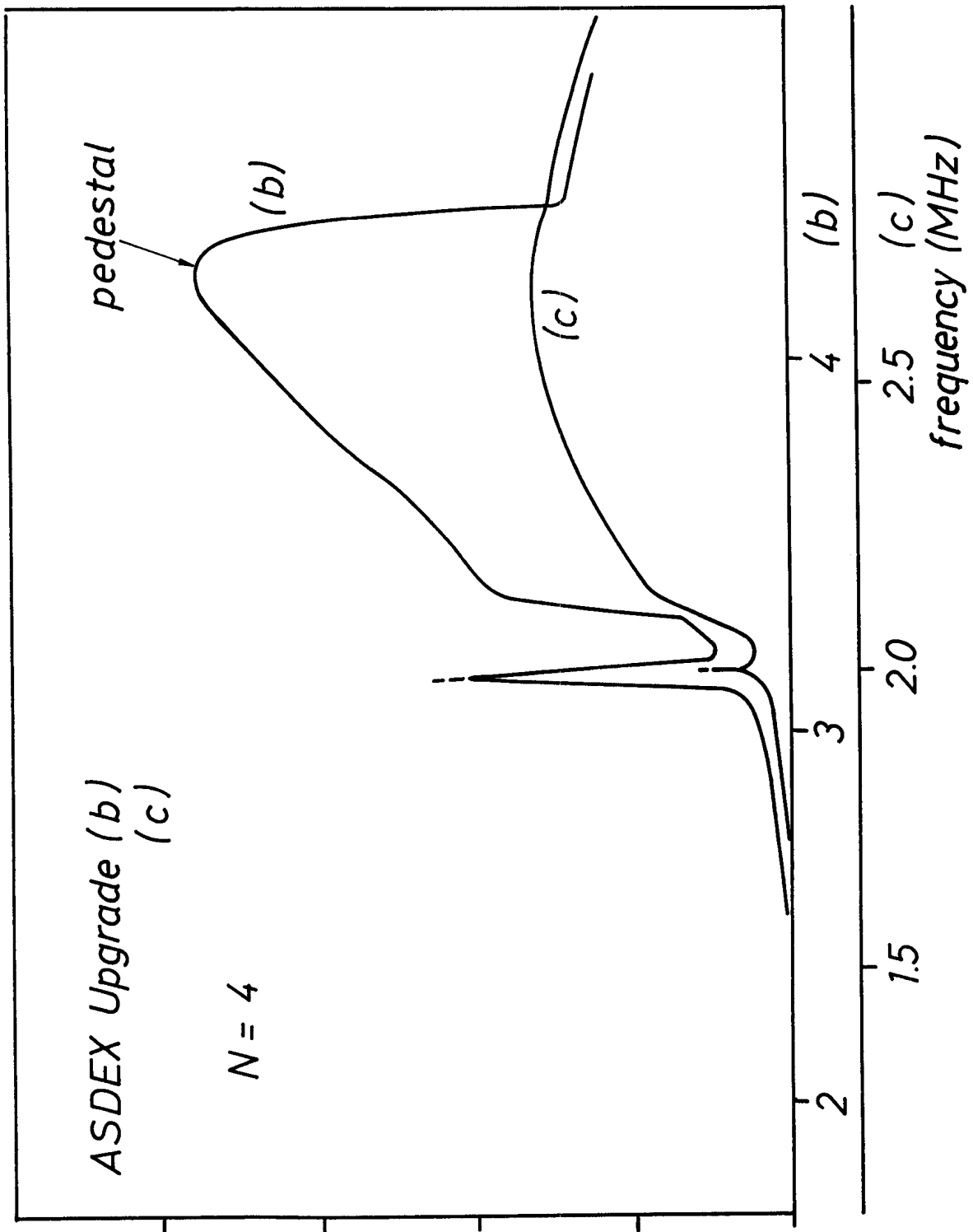
ASDEX Upgrade (b)
(c)
N = 4
pedestal
(b)
(c)
R_{ant} (Ω)
2.0
1.5
1.0
0.5
0
2
3
4
(b)
2.5
(c)
1.5
2.0
frequency (MHz)

Figure 9(a)

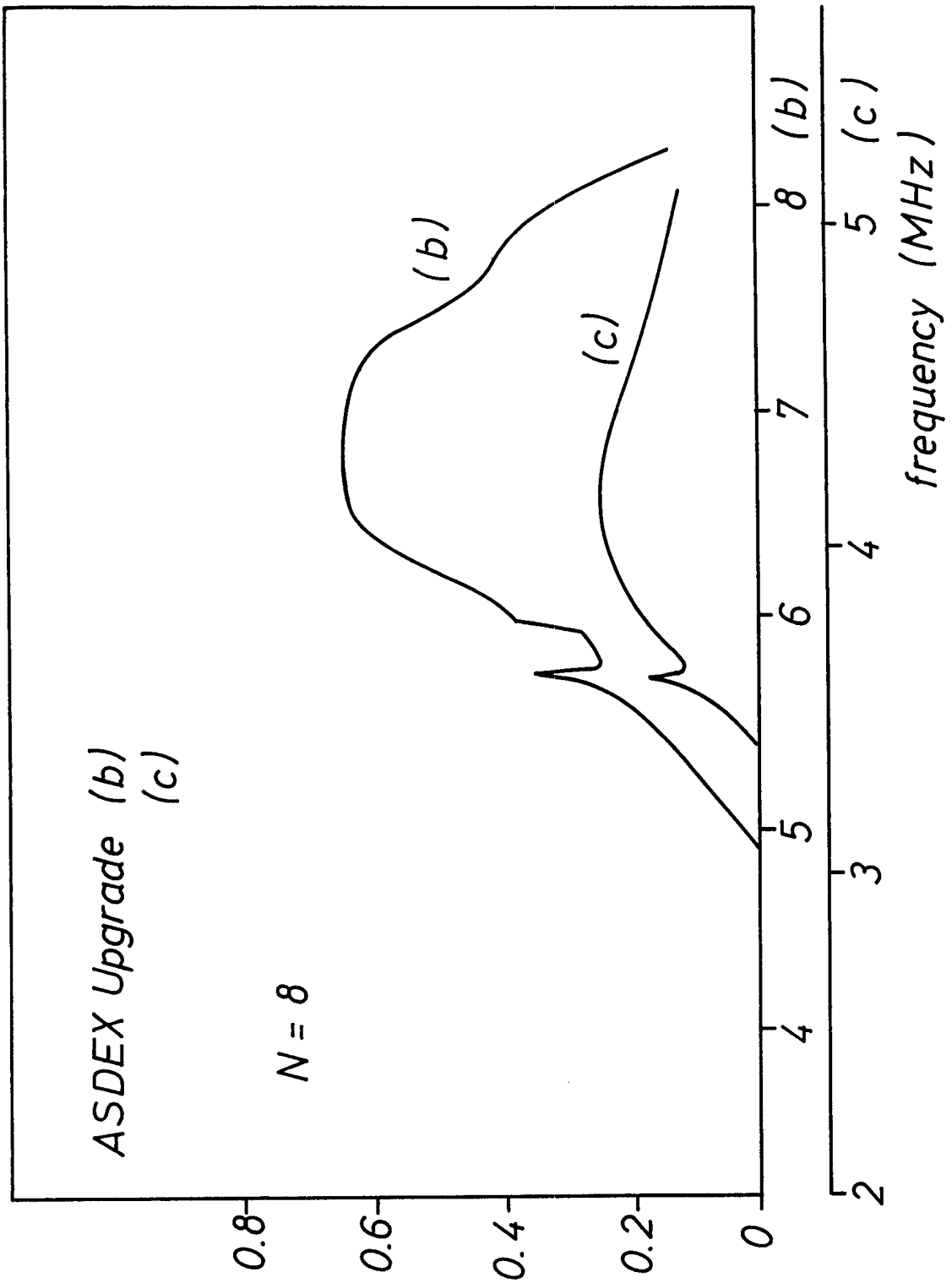
ASDEX Upgrade (b)
(c)
N = 8
(b)
(c)
R_{ant} (Ω)
0.8
0.6
0.4
0.2
0
2
3
4
5
6
7
8 (b)
5 (c)
4
frequency (MHz)

Figure 9(b)

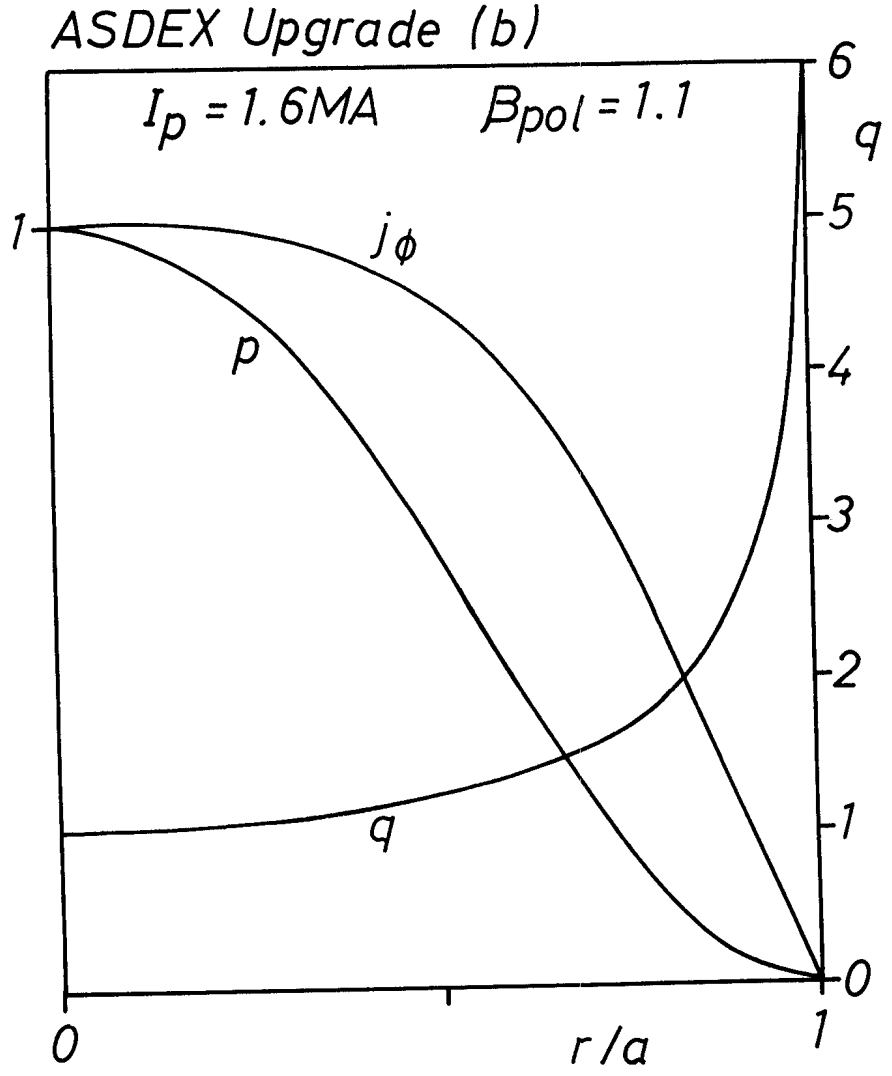
ASDEX Upgrade (b)
I_p = 1.6MA
β_{pol} = 1.1
6
q
5
4
3
2
1
0
1
j_ϕ
p
q
0
r/a
1

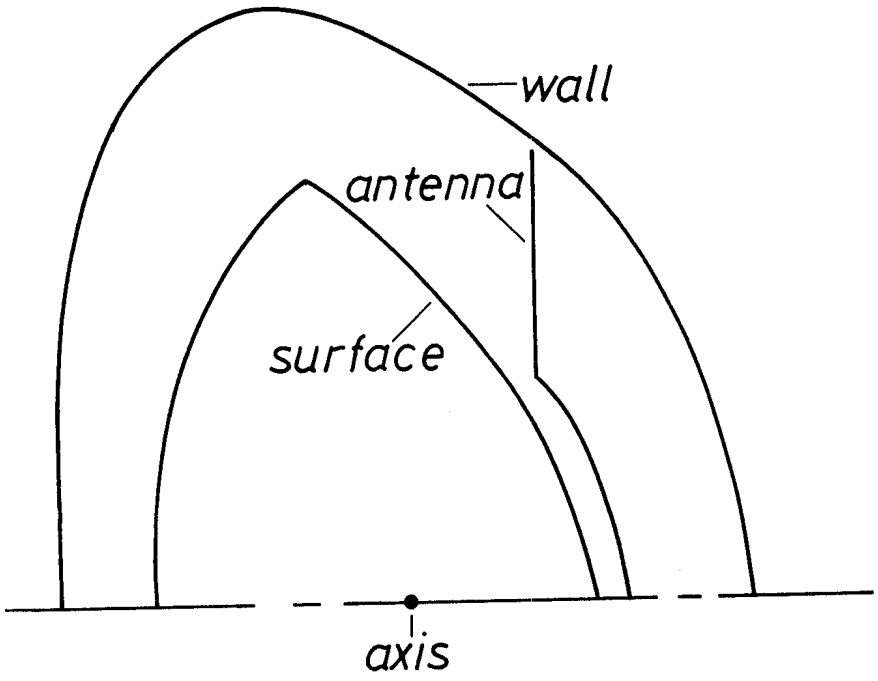
wall
antenna
surface
axis

Figure 10

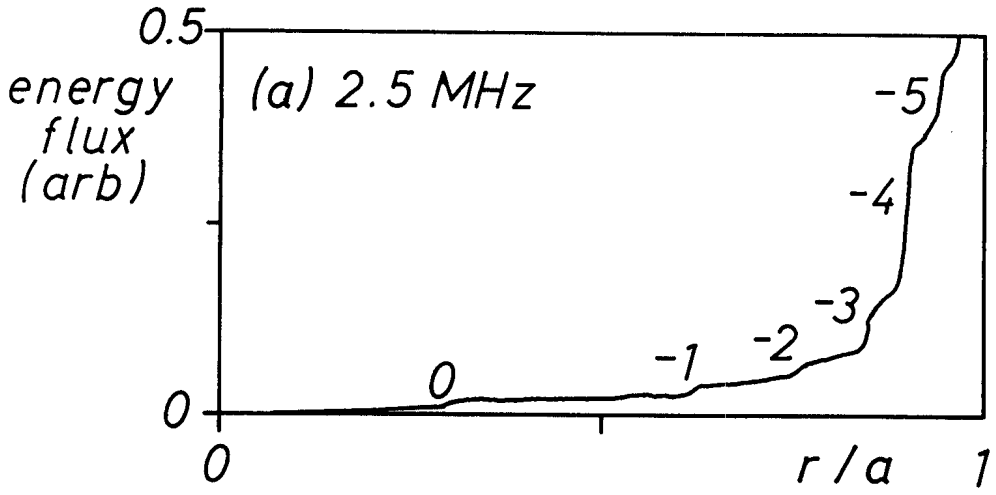
0.5
energy
flux
(arb)
(a) 2.5 MHz
-5
-4
-3
-2
-1
0
0
0
r/a
1

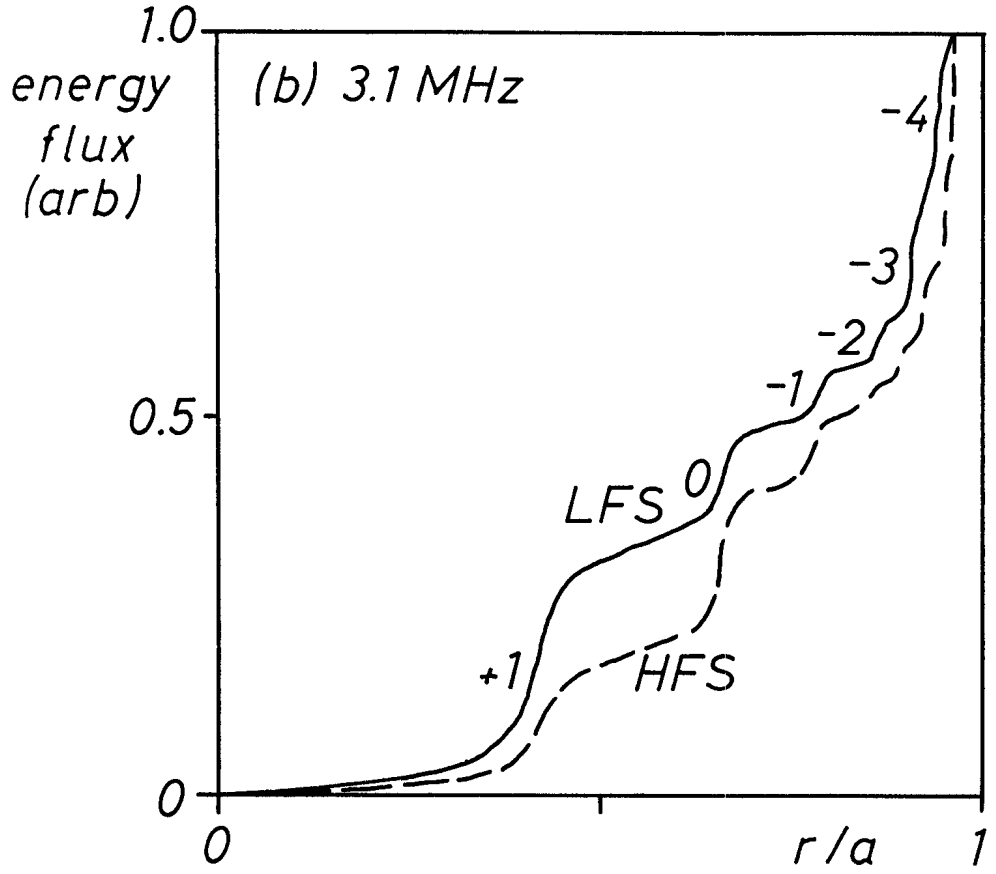
1.0
energy
flux
(arb)
(b) 3.1 MHz
-4
-3
-2
-1
0.5
LFS
0
+1
HFS
0
0
r/a
1

Figure 11

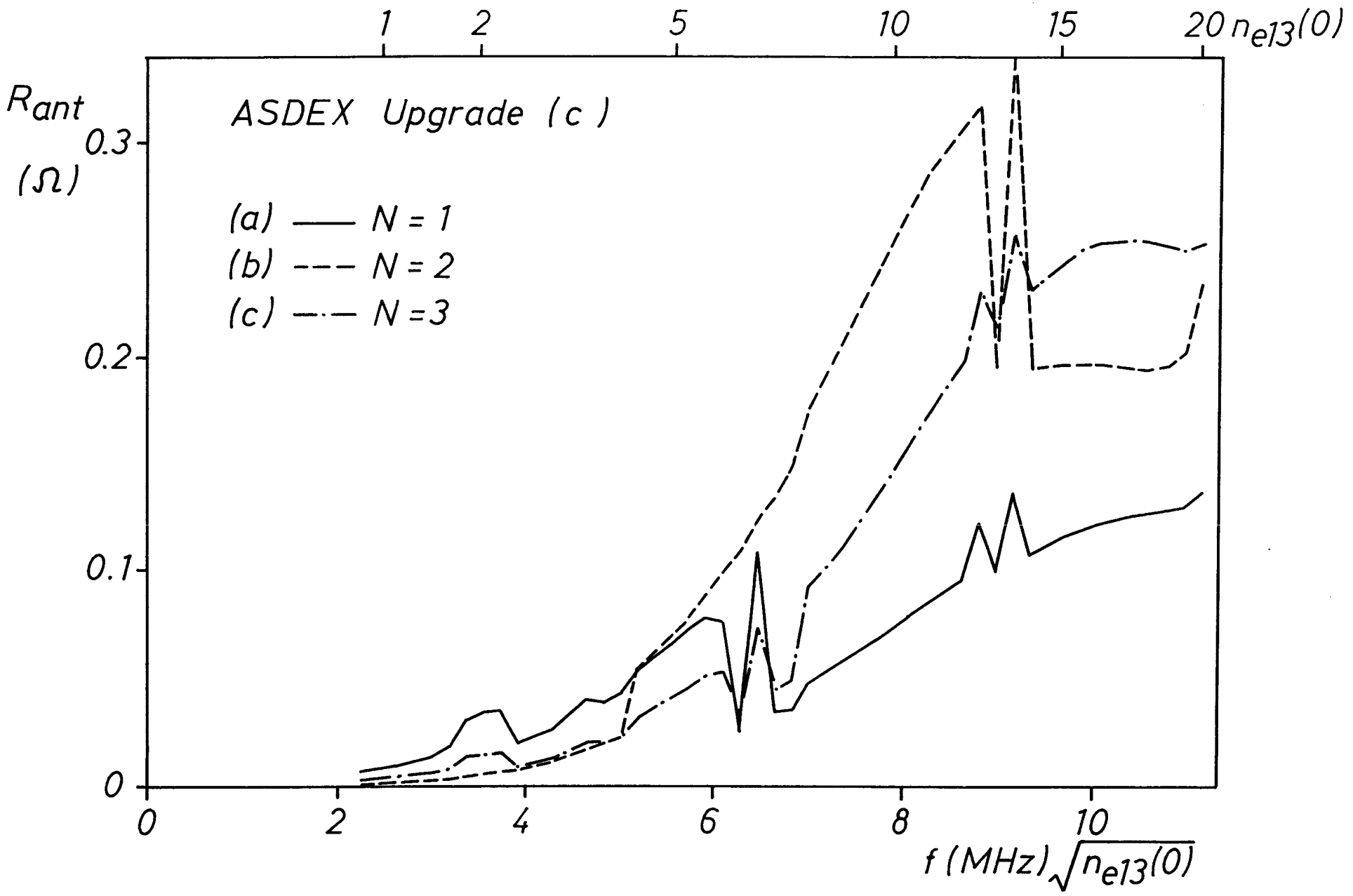
1
2
5
10
15
20 $n_{e13}(0)$
R_{ant}
(Ω)
ASDEX Upgrade (c)
(a) —— N = 1
(b) --- N = 2
(c) —·— N = 3
0.3
0.2
0.1
0
0
2
4
6
8
10
$f\,(MHz)\sqrt{n_{e13}(0)}$

Figure 12

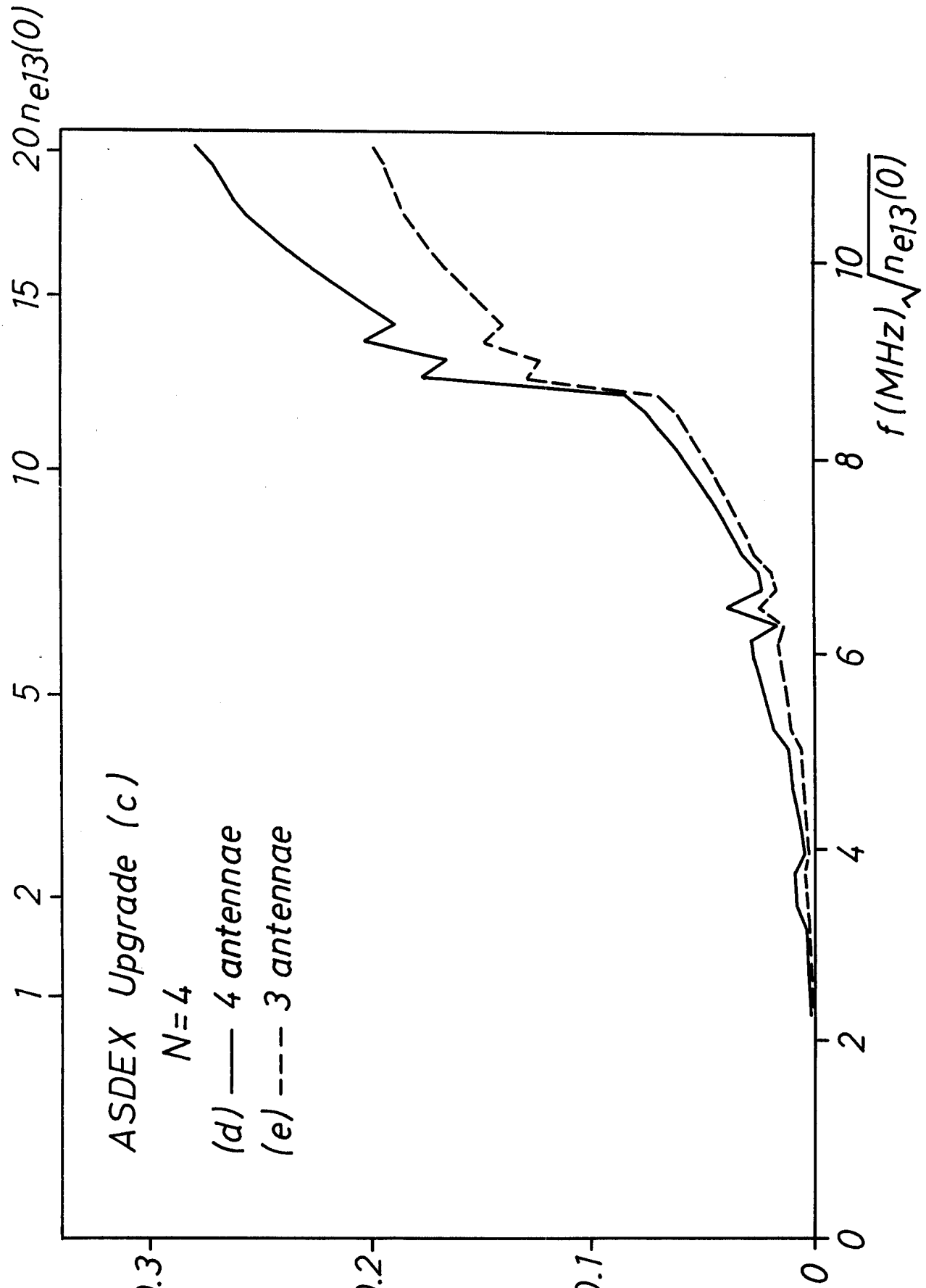

Figure 12(cont.)

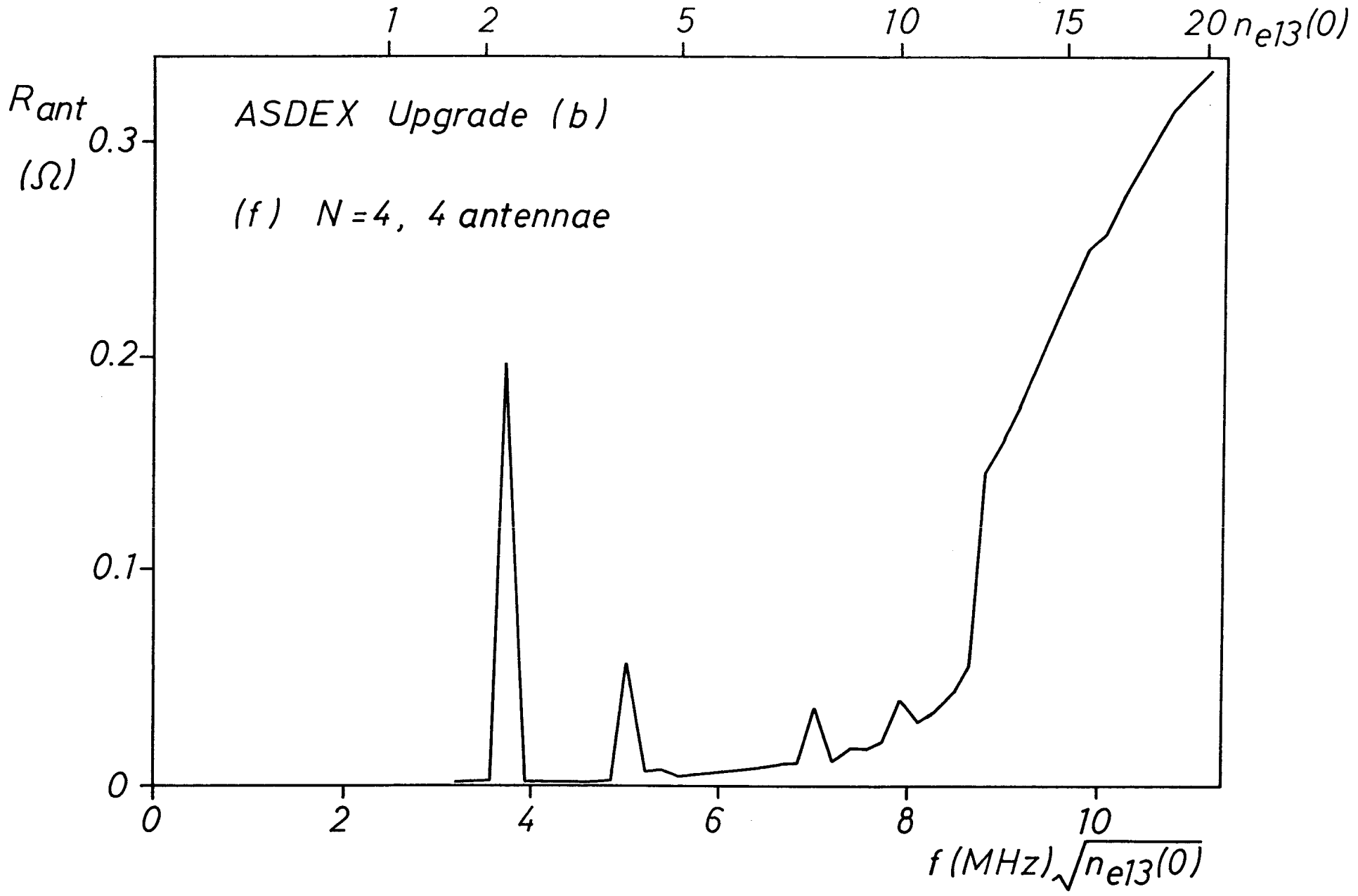

Figure 12(cont.)

ASDEX Upgrade

ONE ANTENNA CIRCUIT

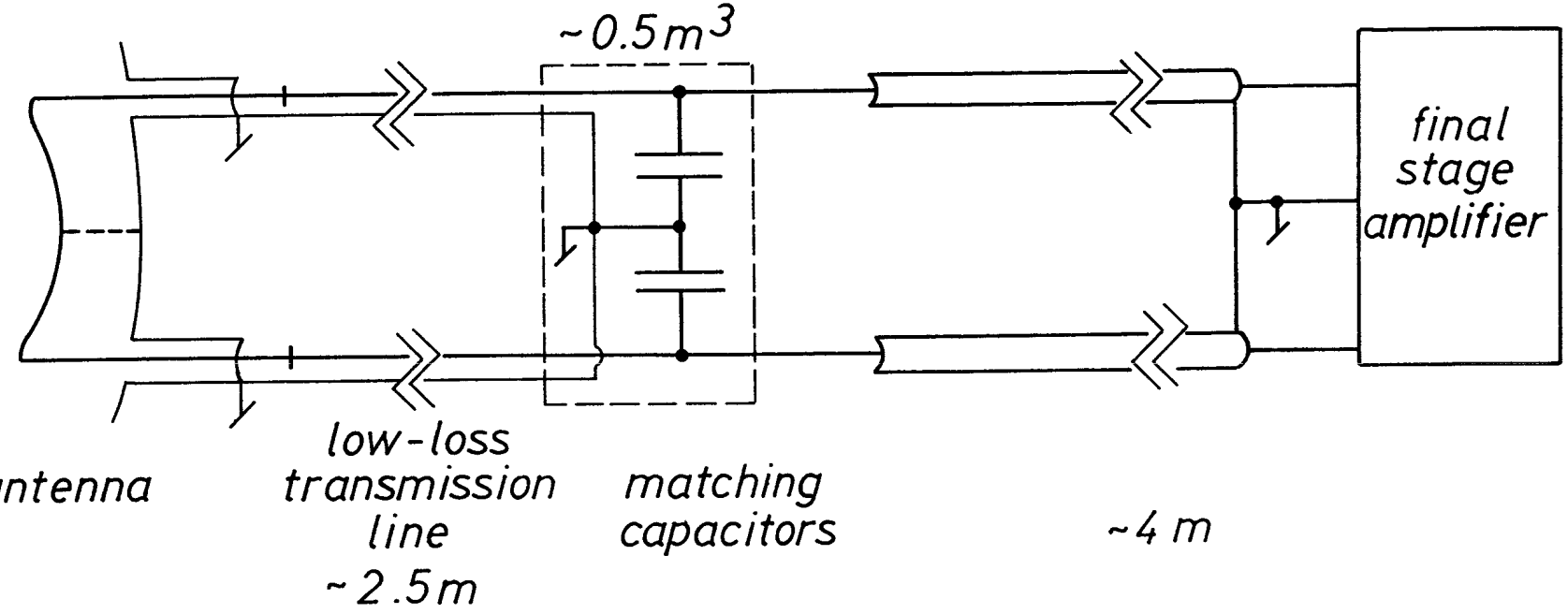

Figure 13